The outdoor field test and energy yield model of the four-terminal on Si tandem PV module

Kenji Araki [1]*, Hiroki Tawa [2], Hiromu Saiki [2], Yasuyuki Ota [3], Kensuke Nishioka [2] and Masafumi Yamaguchi [1]

[1]   Toyota Technological Institute, Nagoya 468-8511, Japan
[2]   Faculty of Engineering, University of Miyazaki, Miyazaki 889-2192, Japan
[3]   Institute for Tenure Track Promotion, University of Miyazaki, Miyazaki 889-2192, Japan
*   Correspondence: cpvkenjiaraki@toyota-ti.ac.jp; Tel.: +81-52-8091830

Featured Application: This technology is expected to be applied to high-performance photovoltaic applications like zero-emission buildings, light-weight aerospace, and possibly, vehicle-integrated photovoltaic.

Abstract: The outdoor field test of the 4-terminal on Si tandem photovoltaic module (specifically, InGaP/GaAs on Si) was investigated and performance model, considering spectrum change affected by fluctuation of atmospheric parameters, was developed and validated. The 4-terminal on Si tandem photovoltaic module had about 40 % advantage in seasonal performance loss compared with standard InGaP/GaAs/InGaAs 2-terminal tandem photovoltaic module. This advantage is expanded in (subarctic zone) < (temperate zone) < (subtropical zone). The developed and validated model used all-climate spectrum model and considered fluctuation of atmospheric parameters, and can be applied every type of on-Si tandem solar cells.

Keywords: photovoltaic; solar spectrum; tandem cell; energy yield model; on-Si tandem; terminal

1. Introduction

High-efficiency is the typical research target of photovoltaic technology. However, it is also known through field experience and theoretical analysis considering spectrum fluctuation that the photovoltaic system that wins the race of efficiency does not always gain the best yield in the real installation [1-4].

Currently, Si solar cell has commonly prevailed in the market. The best efficiency of the Si that was confirmed testing laboratories is 26.7% [5], and the theoretical limit is 29.43% [6]. For further improvement of efficiency, multi-junction or tandem configuration is preferred. The idea of multi-junction cells was suggested [7] and investigated [8] in the early days of photovoltaic technology. The significant progress was triggered by AlGaAs/GaAs tandem cells with tunnel junctions [9] and metal interconnections [10-12]. At that moment, it was predicted that the power-conversion efficiency of multi-junction solar cells would reach close to 30% [13], but this was not fulfilled by difficulties in stable tunnel junctions [14] and defects in the AlGaAs [15]. The break-through was a high-performance, stable tunnel junctions with a double-heterostructure [16]. InGaP was introduced for the top cell [17], and as a result, it was finally achieved to almost 30 % efficiency by a GaInP/GaAs cell [18]. Higher efficiencies have been made with InGaP/GaAs/InGaAs triple-junction cells [19] and with a 5-junction cell [20].

On-Si tandem solar cells use the widely-used Si solar cell as the bottom junction of the tandem solar cell. Because the technology of Si solar cells is well-established, the production cost of the solar cell is expected to reduce, at least, the one to the substrate or the bottom junction [21]. The III-V/Si (III-V on Si) 3-junction and 2-junction tandem solar cells right now exhibit excellent efficiency with 35.9% [22] and 32.8% [22]. The perovskite on Si 2-junction tandem solar cells reached to 28.0% [23]. That of CdZnTe on Si tandem solar cell was 16.8% [24], and GaAs nano-wire on Si tandem solar cell

was 11.4% [25]. The III-V/Si tandem solar cell has the best efficiency among them. Related to this III-V/Si tandem solar cell technologies, several module technologies, including a partial concentrator module [26]. The tested power conversion efficiency of a pair of InGaP/GaAs partial concentrator cell on Si, including optical loss of the concentrator optics, was 27.1% [27]. The partial concentrator module, also using InGaP/GaAs partial concentrator cell on Si and designed for automobile application, showed 21.5% module efficiency [28]. The non-concentrating module using InGaP/GaAs cell on InGaAs by 4T configuration showed 31.17% [1, 29].

Another big group of the candidates of the on Si tandem cells is Perovskite on Si tandem cell. Including a review of the 4T Perovskite on Si cell [30], and challenging on the growth on the textured silicon [31-33]. Related to the topic of this paper, consideration of the performance of the Perovskite on Si tandem cell was done extending the standard testing condition (AM1.5G spectrum and consideration of the diffused sunlight). Still, it was not validated by the annual outdoor operation [34].

Regardless of the material type combined with Si bottom junction, mismatching loss by the spectrum change will be a big issue [35-40]. The intensive studies of the spectral sensitivity of the tandem cell were firstly done in the analysis of the concentrator photovoltaic (CPV) since tandem solar cells were expensive. Still, high-performance and the concentration operation was commercially advantageous to the application [41-50]. The spectrum shift from the standard AM1.5G spectrum destroys the balance of the output electrical current from the sub-cell. Then, the sub-cell with the least output current constrains the total electrical current by the conservation of the carrier or the Kirchhoff's law. It is called "spectrum-mismatching loss." It is an inherent loss for every type of tandem solar cell, regardless of CPV or standard flat-plate application, irrespective of on-Si or on-CIGS tandem, or regardless of III-V or Perovskite tandem solar cells except for more than 3 terminal configurations where the output of the sub-cells is individually connected to the load. It is essential to note that a variation of the solar spectrum by sun height and fluctuation of scattering and absorption of the air by the seasonal effect will affect the annual performance. However, many pieces of research and developments were done to minimize the influence of spectrum change by the improvement of the solar cell design [51-56].

Research and development seeking for the device design with the robustness to spectrum change have been made in the past 20 years, including a computer model named Syracuse by Imperial College London [2, 57-58]. For CPV applications that have been the center of the study of the tandem cells with the robustness of spectrum issues, it was understood that the chromatic aberration of the concentrator optics enhanced the spectrum-mismatching loss [59-63]. However, such loss could be solved by the innovation of optics, including homogenizers and the secondary optical element (SOE) [64-65]. The remaining problems of the spectrum-mismatching loss have been overcome by the adjustment of the spectral response of each sub-cell, including overlapping the absorption spectrum and broadening the absorption band to the zone of massive fluctuation.

The model, theory, and advanced design of CPV, as well as innovations for solving the issue of the spectrum loss in the real-world solar irradiance, were tried to be validated by the outdoor energy yield monitoring. However, it was not very successful. One possible reason was the performance of CPV was also sensitively affected by the tracking error and misalignment of the concentrator optics and the solar cell. However, this issue was solved by the series of innovations of the testing method of the misalignment [66], validation in the production line of the CPV module [67], and the analysis of the impact on the energy output [68-69]. After solving uncertain factors, the influence of the spectrum change was re-examined. However, it was found that the standard model using air-mass (or the sun height) as the parameter of the solar spectrum, which has been used by many scientists and for more than 20 years, could not explain the seasonal trend of the performance by analysis [70] and the same results using variance (ANOVA) [71]. The new-findings that directly and more strongly influence the spectrum than the air-mass was a fluctuation of atmospheric parameters. This was because the impact by the sun-height appears strongly when the airmass value is more than 2. And both summer and winter have the early morning and the late evening time equally. Namely, without

consideration of atmospheric parameters, it is next to impossible to predict the annual energy yield, in other words, it is next to impossible to design the optimal tandem solar cells in yearly energy yield.

Recently, tandem solar cells have been considered for use in non-concentrating applications, out of CPV, including vehicle-integrated photovoltaic (VIPV) and car-roof photovoltaics (PV) [72-84]. It was thought that most electric vehicles (EV) might be able to run by solar energy using tandem cells on the car roof [1]. The area of the car roof and other car-bodies are limited. Moreover, solar cells cannot be laminated to an undevelopable curved surface of the car body. It is difficult to cover the restricted area of the car-roof surface entirely. Therefore, extremely high performance that can be brought by tandem solar cells is highly required.

The analysis of the spectrum sensitivity on CPV was done in our previous research [85-86]. The calculation and analysis for CPV were more straightforward because we did not have to consider angular effects combined with the mixture of the direct and diffused components of the sunlight. Different from CPV applications that the cell is always perpendiculary illuminated by the sun using a solar tracker, and only utilizes the direct sunlight, the typical application needs to use a diffused component of the sunlight from the sky, ground reflection, and skewed solar rays, with a combination of direct and diffused elements as a function of the sun orientation relative to the solar panel orientation. For an extension to non-concentrating applications, we need to solve the complicated coupling of spectrum and angles (Table 1). The key parameters are atmospheric parameters that are dependent on each other. For example, different incident angle modifier and different orientation lead to a diverse mixture of direct and diffused sunlight.

Table 1. The difference in performance modeling between CPV and standard installation [1]. The outdoor performance of CPV was intensively studied in more than 20 years considering spectrum mismatching problem of the tandem solar cells.

	CPV [1]	Normal Installation
Solar spectrum	Only direct	A mixture of direct, diffused from the sky, and reflection
Angle	Always normal	Varies by time and seasons
Spectrum by angle	Constant (only normal)	Needs consider coupling to angle

[1] It only generates power only by direct solar irradiance using a 2-axis solar tracker.

Four-terminal (4T) tandem cells were designed so that the output of the Si cell and other top junctions were taken independently, thus robust to the spectrum change. In the case of III-V/Si three-junction solar cells that are frequently considered as an excellent candidate for the high-efficiency solar cells, the output terminal from the top cell comes from two-junction III-V solar cells, and the top two-junction cell is still susceptible to spectrum change. Therefore, a long-term field test of the module using III-V/Si 4T solar cells is essential to the validation of the use of this configuration. Currently, the best efficiency confirmed by the third-party is 33.3% [87].

Other groups of the 4T type tandem cells are partial concentrator cells and 3T tandem cells. The partial concentrator solar cell was first proposed in 2017, using wide-acceptance concentrator optics that selectively concentrate onto the top III-V cells stacked on the larger size Si bottom cell. This type of the tandem solar cell was considered to the application to VIPV [89] and various design method and modeling were invented [90-92]. Several prototypes were made [79] and as high as 27.4 % of annual average efficiency was anticipated [78]. 3T type tandem cells are basically connecting one of the terminals of the pairs of two-terminal. This method has an advantage of simplifying the interconnection of the solar cells among the PV module. Several types of the tandem cells, including Ge-based III-V cell [93], polymer type [94], III-V monolithic [95], and III-V on Si [96]. It was also studied advantage of the better spectrum matching operation using this 3T configuration [97].

The background of this study and our motivation are summarized as follows:

1. Tandem solar cells are high-efficiency, and various types of the device structure were studied. On-Si tandem is one of them and it has a distinct advantage of the cost using well-established Si solar cell technology.

2. Regardless of the type of the materials, the annual performance of the tandem solar cells does not perform well by the spectrum mismatching loss.

3. The modeling of the spectrum mismatching loss was studied relying on the airmass variation. The intensive study on CPV performance in more than 20 years revealed that the fluctuation of atmospheric parameters played essential role.

4. Due to the development of the new application of the high-efficiency solar cell, including vehicle-integrated solar cells, the precise annual energy yield modeling of the tandem solar cells are demanded. The knowledge in precise spectrum-mismatching modeling in CPV is expanded to the non-concentration standard installation.

5. 4T on Si tandem solar cell is a good candidate for the robustness to the spectrum variation. Its outdoor operation and energy yield modeling was intensively studied in this article. The model did not rely only on airmass, but considered real fluctuation of the spectrum in all kind of climate considering atmospheric fluctuation.

2. Methods

The purpose of our work is to develop an accurate way of predicting the performance of photovoltaic modules using tandem 4T solar cells, considering spectrum variation. The base model of the spectrum is Bird's model [98]. Bird's model only covers the clear sky days, and we expanded it to cover all-climate roughly [99]. This new spectrum model and the response of the tandem module was validated by the long-term (multiple years) measurement of the performance of the module [99].

2.1. Device configuration

The fundamental difference of 2T and 4T configuration is that the former one connects entire sub-cells all in series, and the latter divides the circuit into two pieces using two-pairs of output lead, namely, four-terminal (Figure 1). Each pair of leads can be connected to two independent loads so that each 2T output can be controlled by independent MPPT (maximum power point tracking). There are two advantages. One is less loss in spectrum mismatching because the shorter-wavelength zone and longer-wavelength zone are connected independent loads. Another is more flexibility in the design of the solar cell. In this particular case, the 4T configuration uses Si to the bottom sub-cell and III-V two-junction cell in the top sub-cell. Both sub-cell technologies are well-established, and it is not necessary to consider various constraints of the integration into one-piece (typically monolithic growth) solar cells.
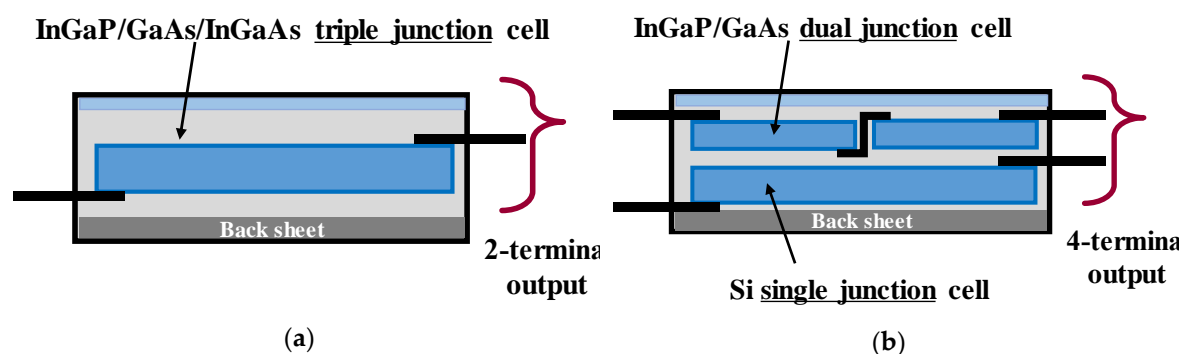
Figure 1. Measured 4T III-V/Si module and its solar cell structure: (**a**) Description of 2-terminal III-V 3-junction module; (**b**) Description of measured 4T III-V/Si module, 2 + 1 junctions. Note that the number of junctions is the same

2.2. Measurement system

The field test was done at the University of Miyazaki. The details of the measurement setup can be found in our recent publication of Applied Sciences [99], as shown in Figure 2.

The module with InGaP/GaAs two-junction cell on Si solar cell was provided by SHARP and tested at the University of Miyazaki simultaneously with a 2T three-junction module (InGaP/GaAs/InGaAs). An I-V curve tracer measured the performance of these two PV modules. Pyranometers were placed on 25° (EKO MS-602) and 35° (EKO MS-411) in the slope angle to measure global irradiance. Another pyranometer was installed on a two-axis sun-tracking (EKO MS-602) to measure global normal irradiance. Every 3 minutes, the irradiance of these sensors was captured and logged from 5:30 a.m. to 6:30 p.m. The solar spectrum, specifically the global spectrum on the sloped surface, was measured by the spectro-radiometers (EKO MS-711, MS-712). Their slope angles were 35°. Measurements of the global spectrum were every 10 min from 5:00 a.m. to 8:00 p.m.

2-terminal InGaP/GaAs/InGaAs	4-terminal InGaP/GaAs on Si
(**a**)	(**b**)
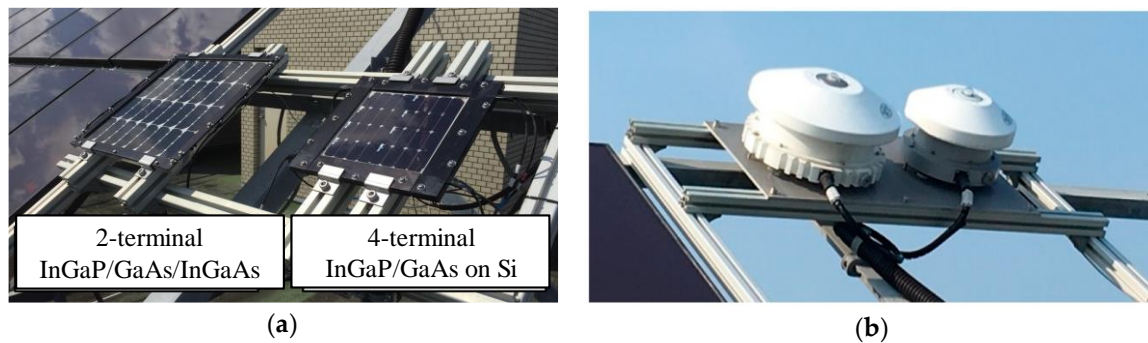
Figure 2. Measured 4T III-V/Si module and its solar cell structure: (**a**) Description of measured 4T III-V/Si module, 2 + 1 junctions (right) with comparison to the 2-terminal III-V 3-junction module. Note that the number of junctions is the same; (**b**) Spectro-radiometers [99].

2.3. Spectrum model

The performance model we used was identical to the one we used to analyze the PV module using the 2T configuration [99]. We called it an MS2E model (Miyazaki Spectrum-to-Energy method). Let us describe a rough flow of the analysis and the model.

First, we need to define the solar spectrum. The spectrum we assumed was a linear combination of the spectrum of the clear sky condition and that of the overcasting state [99]. The spectrum of the overcasting state was assumed that the solar power was lost just by absorption, corrected by the solid angle of the sky influenced by the slope angle of the module. Then, the global solar spectrum is approximated as Equation (1) and Equation (2).

$$I_\lambda = f I_{1\lambda} + (1-f) I_{2\lambda} \tag{1}$$

$$f = \frac{DNI}{\int_{300\,nm}^{4000\,nm} I_{d\lambda} d\lambda} \tag{2}$$

where, I_λ is the global spectral irradiance calculated by our spectrum model covering all-weather at a wavelength. The unit of I_λ is W/m²nm. f is the weather correction factor defined by Equation (2), $I_{1\lambda}$ is the global spectral irradiance calculated using Bird's spectrum model [98] at a wavelength. The unit of f is W/m²nm. $I_{2\lambda}$ is the global spectral irradiance calculated by a spectrum model assuming full cloud covering the sky at a wavelength. The unit of $I_{2\lambda}$ is W/m²nm. DNI is the direct normal irradiance. And, $I_{d\lambda}$ is the direct normal solar spectral at a wavelength. The unit of $I_{d\lambda}$ is W/m²nm. The spectrum calculated by this model, with contrast to Bird's model is shown in Figure 3 [99]. Note that the Bird's spectrum model was improved by considering atmospheric parameter variability. The Y-axis corresponds to the normalized global spectrum irradiance by integrated spectral irradiance. The black trend line is measured and normalized global solar spectral irradiance. The gray trend line is the reference spectrum in AM 1.5G. The red trend line and the blue trend line are the calculated global solar spectral irradiance by the MS2E method. Note that Bird's model only considers air mass, namely, the atmospheric parameters are constant. In the wintertime, atmospheric parameters are close to those under the standard conditions, so that the estimated solar spectrum approaches to the

reference AM1.5G spectrum. In the summertime, the aerosol density often drops than that of the standard value, and the precipitable water grows larger. The short-wavelength region of the solar spectrum becomes fat, and the long-wavelength part becomes thin. During the cloudy days, the influence of cloud appears in the short-wavelength part of the solar spectrum so that the long-wavelength region drops.
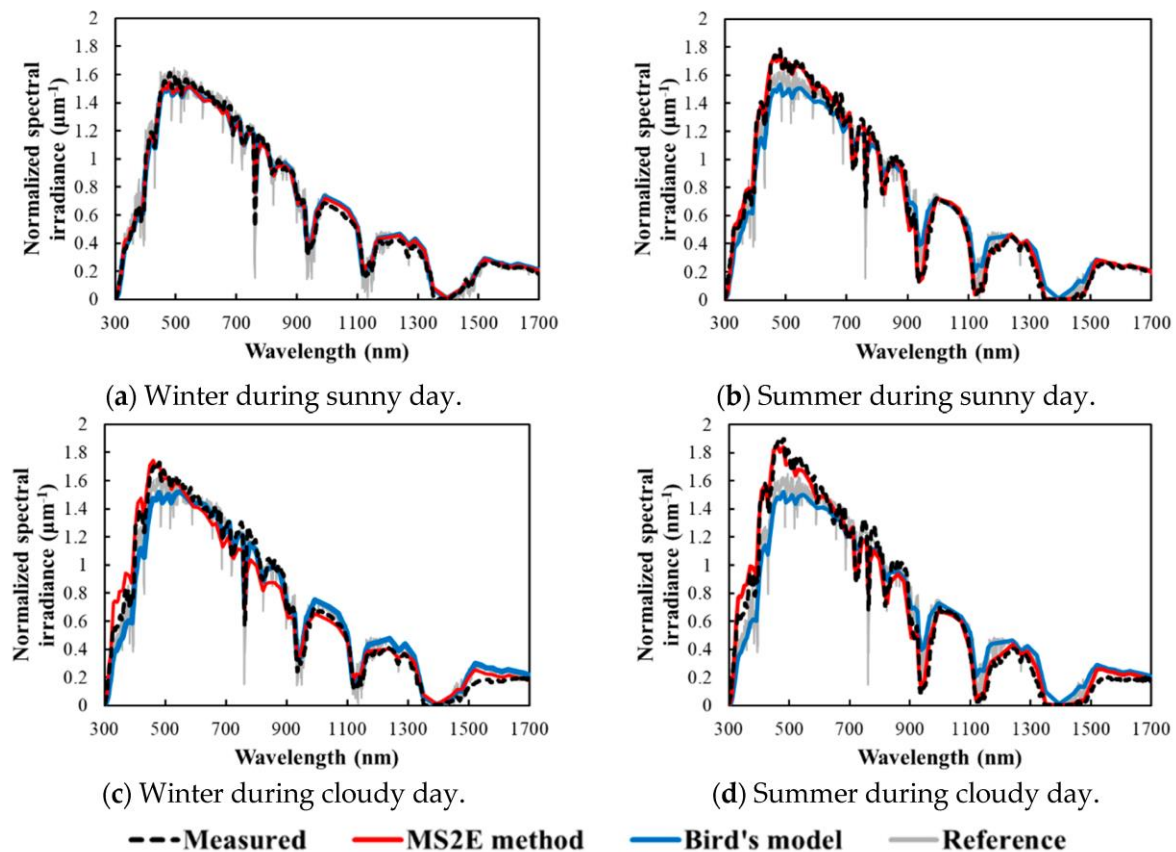
Figure 3. Comparison with measured and estimated values (Bird's model and MS2E model) of global irradiances tilted at 35° [99].

Figure 4 indicates the measured aerosol density and precipitable water by the curve fitting to the measured solar spectrum. The aerosol optical depth was much lower than the standard value used to the calculation of the reference spectrum in summer (Figure 4 (a)). This is why the measured and estimated irradiances in the summertime are high than that of global irradiances (AM 1.5G) at the wavelength range of 450-550 nm. The precipitable water was much higher than the standard value used to the calculation of the reference spectrum in summer (Figure 4 (b)). This is why the measured and estimated irradiance dips are broader than that of global irradiances (AM 1.5G) at the wavelength range of 1350-1450 nm and around 1150 nm.

(a) Aerosol optical depth   **(b)** Precipitable water
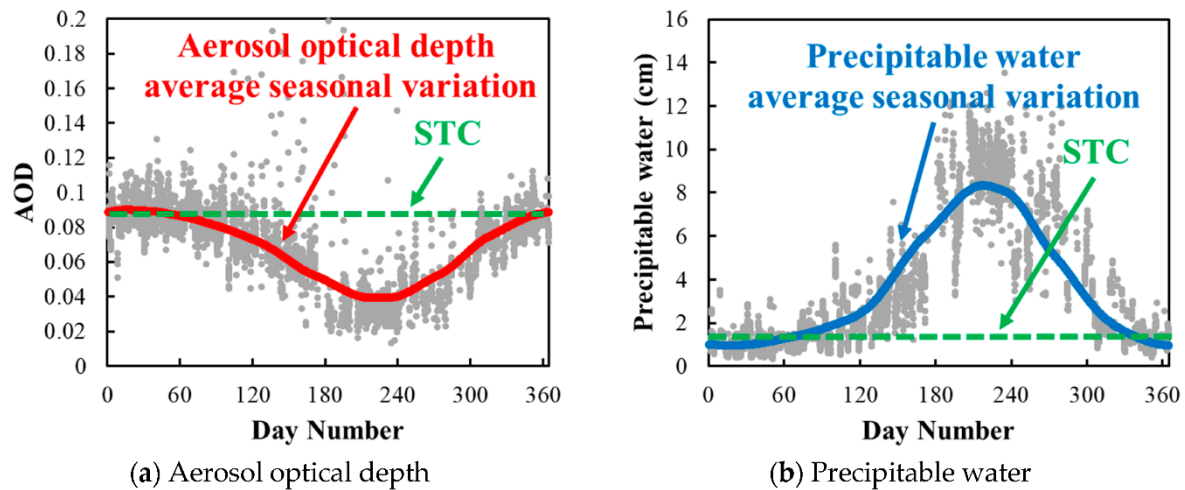
Figure 4. Seasonal trend of atmospheric parameters in Miyazaki [99].

2.4. Performance model

The power output of the module is the product of the short-circuit current, open-circuit voltage, and fill factor (*FF*). First, *FF* was calculated by the ratio of the spectrum mismatching. The calculation step is as follows. First, generating a correlation chart between calculated *FF* and the ratio of mismatching at first using random numbers. Then, the trend curve of these two parameters was fitted to the parabolic. Finally, the *FF* was represented as the function of the spectrum-mismatching ratio. The short-circuit current can be calculated as the integral of the product of the spectral irradiance and spectral efficiency of the module, which can be derived from the external quantum efficiency affected by spectrum mismatching. The angular characteristics in the photon absorption were measured in advance. The detailed calculation procedure was identical to our previous work [99].

We also needed to consider the coupling between spectrum and angles. The atmospheric parameters are dependent on each other. For example, a combination of the incident angle modifiers and the orientations results in a diverse mixture of the direct and the diffused sunlight. The atmospheric parameters were calculated by the spectrum, by a data-fitting calculation called the Bird's model [100-101] at the University of Miyazaki [102]. The model for this analysis is given in Figure 5 [1]. The nonlinear effect result from distributed effects often seen in III-V (especially concentrator cells) was not considered [103-105].
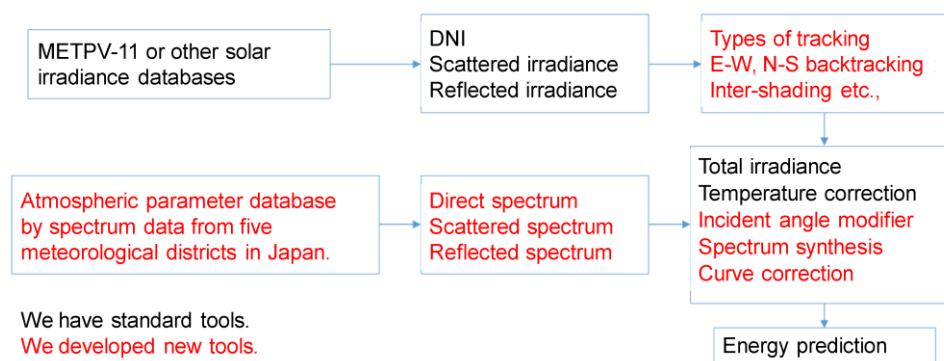
Figure 5. The performance model of the tandem solar cells, considering the spectrum and angle interaction [1].

3. Results

First, we examined our performance model (MS2E model) that could be applied to the PV module using 4T tandem cells. We monitored the module performance in every 3 minutes from 05:30 to 18:30 on January 3, 2019. The slope angle was 35°. The location of the test site at the University of Miyazaki was N31.83°, E131.42°. The result of the measurement and the validation result is shown in

Figure 6 and Table 2. The output trend in Figure 6 was decomposed to InGaP/GaAs top cell and Si bottom cell, namely, we applied independent MPPT (maximum power point tracking) search to each pair of the terminals. The predicted output of the 4T tandem module using our MS2E performance model supported by the all-climate spectrum model (Equation (1) and (2)) matched well. It was also shown that the accuracy in prediction of the daily energy yield is within plus or minus 2% of error.
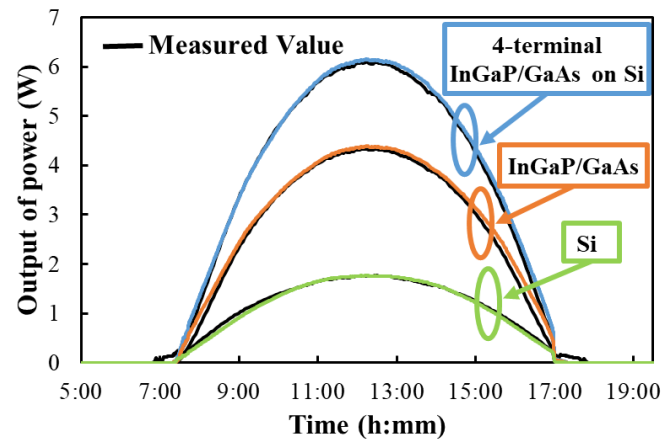
Figure 6. Validation of the performance model (MS2E model) to 4T tandem module, decomposing performance in each output terminal (InGaP/GaAs top cell, and Si bottom cell).

Table 2. Comparison between measured and estimated (predicted by MS2E model) energy yield in a day (January 3, 2019)

	Measured	Estimated	Error
InGaP/GaAs on Si[1]	39.6 Wh	40.4 Wh	1.9 %
InGaP/GaAs	28.0 Wh	28.9 Wh	3.4 %
Si	11.6 Wh	11.4 Wh	1.9 %

[1] 4T configuration independently takes the output from the top and bottom cells; the production of the InGaP/GaAs on Si module is a simple sum from the InGaP/GaAs top layer and Si bottom layer.

4. Discussion

It was shown that our MS2E model is sufficiently accurate to discuss the annual and outdoor performance of 4T tandem modules. Next, let us discuss and compare with other types of tandem modules with consideration of regional variations.

4.1. Comparison between 4T and 2T configuration

The annual performance of the 4T tandem module was calculated by the validated MS2E model. For comparison robustness to the seasonal spectrum change, it is essential to introduce a normalized scale of the performance, because the area, nominal output, cell type, and power conversion efficiency are different. We used performance ratio PR and the ratio of the performance peak-to-peak R_{pp} that is defined by Equation (3) and Equation (4).

$$PR = \frac{(Outdoor\ efficiency)}{(Efficiency\ measured\ by\ STC)} \tag{3}$$

$$R_{pp} = 1 - \frac{(peak\ to\ peak\ of\ PR\ in\ 4T)}{(peak\ to\ peak\ of\ PR\ in\ 2T)} \tag{4}$$

Note STC means the standard testing condition. PR value given by Equation (3) corresponds to how much power generation performance of the photovoltaic module drops in outdoor operation about the indoor testing result measured by the standard testing condition. R_{pp} value given by Equation (4) corresponds to the degree of suppression of the seasonal variation of performance of 4T configuration relative to standard 2T configuration. Both PR and R_{pp} values were integrated

throughout a day, and their daily trend was plotted in time-series. The result with contrast to 2T configuration is shown in Figure 6 and Table 3. Note that the peak-to-peak value of the *PR* variation of 4T configuration was 0.084, and that of 2T was 0.139. The degree of improvement of seasonal variation R_{pp} was 39.8 % (Figure 7 (a)). As a result, the annual energy yield per nominal power of 4T configuration increased to 1500 kWh/kW, and that of 2T was 1442 kWh/kW (Table 3). The improvement was mainly seen in the summer. It corresponded to the variation of water precipitation (Figure 7 (b)). The bandgap of the bottom cell of Si is 1.11 eV, and the absorption edge is 1100 nm so that the performance of the Si bottom cell would not be affected by the water absorption typically seen in around 1200 nm.

(a)   (b)
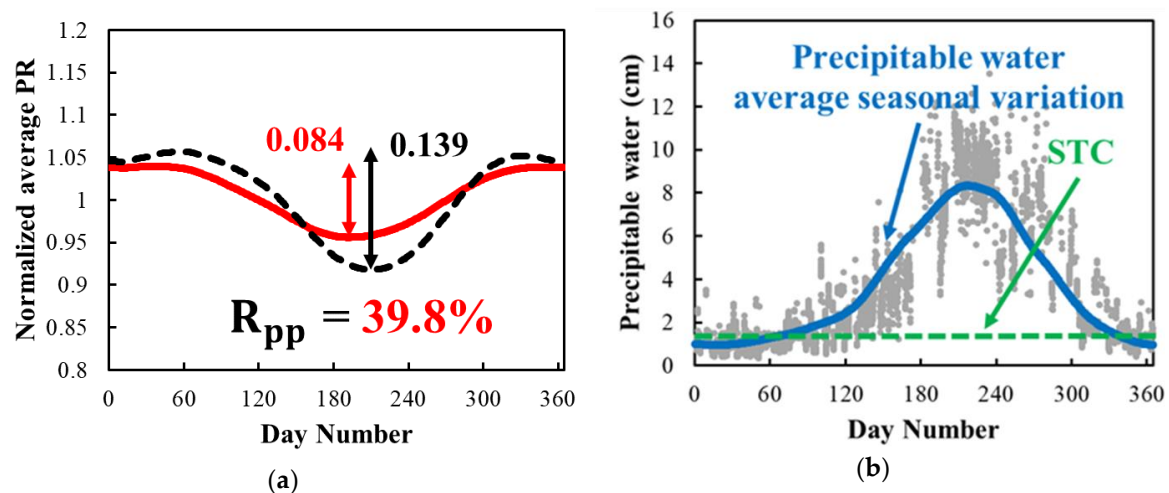
Figure 7. Comparison of the annual output between 4T configuration and 2T configuration affected by the variation of the atmospheric parameter: (**a**) Predicted seasonal fluctuation of the normalized energy yield of 4T (red and solid line) and 2T (black and dashed line) configuration; (**b**) Seasonal variation of precipitable water (optical depth) in our measurement that is likely to be responsible from the difference of behavior between 2T and 4T configuration. Note that this chart is identical to Figure 4 (b) [99].

Table 3. Summary of the outdoor performance of 4T on-Si tandem solar cell and normal 2T three-junction tandem solar cell

	PR peak to peak value	Annual energy yields (kWh/kW)
InGaP/GaAs on Si[1] **(4-terminal configuration)**	0.084	1500
InGaP/GaAs/InGaAs **(2-terminal configuration)**	0.139	1442

[1] 4T configuration independently takes the output from the top and bottom cells; the production of the InGaP/GaAs on Si module is a simple sum from the InGaP/GaAs top layer and Si bottom layer.

On the other hand, InGaAs bottom cell with 1.0 eV bandgap is affected by the absorption of this band. In 2T configuration, the reduction of absorbed photons in this water band constrains the current output of series-connected entire junctions. In addition to the difference in numbers of terminals (4T or 2T), the difference of the bandgap of the bottom cell affected the degree of the seasonal variation.

4.2. Regional difference in the behavior of 4T and 2T performance

The fact that the annual change is affected by water precipitation implies that the gain by 4T configuration may be strongly influenced by the local climate.

With the validation of the MS2E model in the estimation of PV output, we applied it more broadly. The solar database METPV-11 [106-107] has a solar irradiance measurement dataset for more

than 800 sites in Japan. We examined the seasonal energy yields in various locations with different climates. For the determination of the atmospheric parameters, measurement data of the solar spectrum are needed. NEDO classified Japan into five different solar radiation climate zones to clarify regional differences in solar irradiation conditions. The global solar spectrum was monitored at five sites, including Naganuma (Subarctic zone), Tosu (Temperate zone), and Okinoerabu (Subtropical zone). We extracted aerosol density and water precipitation in each solar radiation climate zone. Correctly, the aerosol density and water precipitation were derived using a model in Equation (1) and (2) that minimizes the deviation of the global spectrum between the experimental values measured and the values. Note that the estimated global spectrum is a function of the variables aerosol density and water precipitation [99].

The result is shown in Figure 8. From left to right column, transition from the subarctic zone, temperate zone and subtropical zone, water precipitation, that were calculated by optical absorption of the spectrum using the method as mentioned above, increased. The gain of 4T configuration (R_{pp} value) increased accordingly.
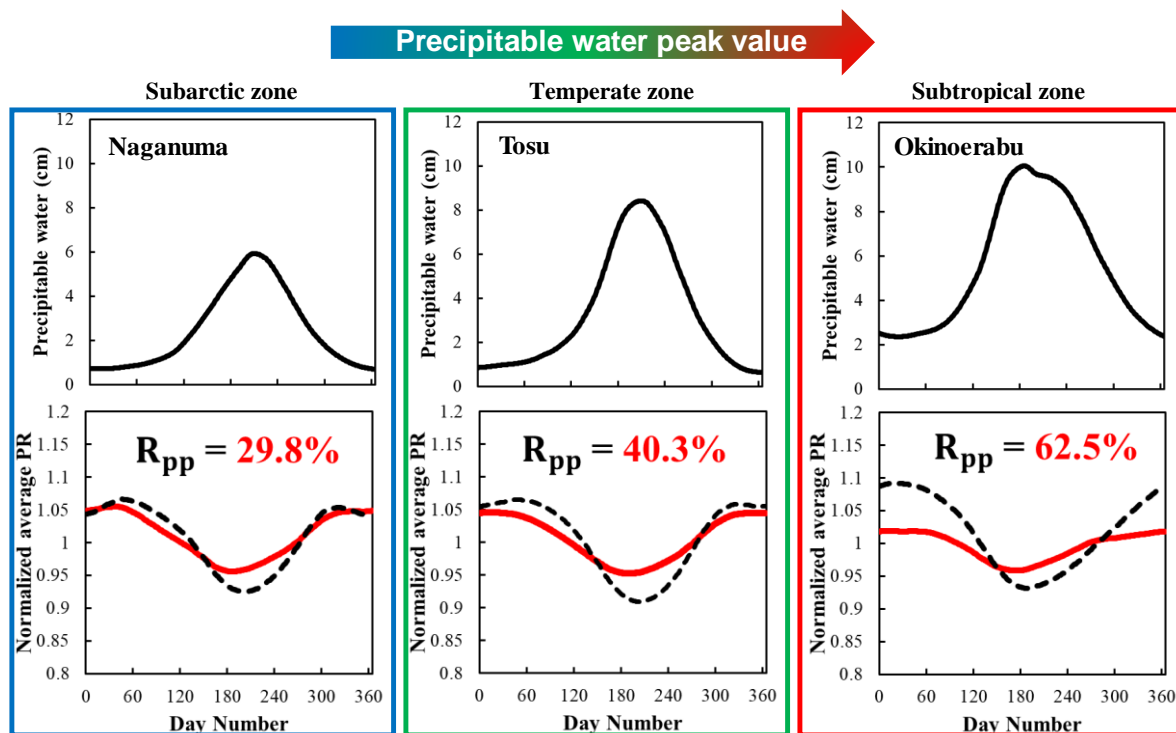
Figure 8. Comparison of the annual output between 4T configuration and 2T configuration affected by the variation of the atmospheric parameter. The red solid trend line in the bottom charts corresponds to the normalized energy yield of 4T, and the black dashed trend line corresponds to that of 2T configuration.

4.3. Further performance improvement

Although the 4T configuration effectively improves the seasonal loss of multi-junction modules, there still is some annual drop. It is because the top cell has two junctions, and its spectrum mismatching drops the output of the top cell.

Further improvement of the mismatching was proposed in several articles. One is fine-tuning of the bandgap energy [108]. The second is enhancing radiative coupling that was shown in the concentrator PV application [109] and non-concentrating application [1].

5. Conclusions

Tandem solar cells are high-efficiency, and various types of the device structure were studied. On-Si tandem is one of them and it has a distinct advantage of the cost using well-established Si solar cell technology. Regardless of the type of the materials, the annual performance of the tandem solar cells does not perform well by the spectrum mismatching loss. The modeling of the spectrum mismatching loss was studied relying on the airmass variation. The intensive study on CPV performance in more than 20 years revealed that the fluctuation of atmospheric parameters played essential role. Due to the development of the new application of the high-efficiency solar cell, including vehicle-integrated solar cells, the precise annual energy yield modeling of the tandem solar cells are demanded. The knowledge in precise spectrum-mismatching modeling in CPV is expanded to the non-concentration standard installation. 4T on Si tandem solar cell is a good candidate for the robustness to the spectrum variation. Its outdoor operation and energy yield modeling was intensively studied in this article. The model did not rely only on airmass, but considered real fluctuation of the spectrum in all kind of climate considering atmospheric fluctuation.

Many previous studies tried to calculate the spectrum conditions only by airmass and also tried to apply the model that was developed for the clear-sky conditions. The airmass based calculation was proved inaccurate in the intensive investigation to CPV modules using three-junction tandem cells. The lack of all-climate spectrum model was not the issue for the application to CPV, because it only used the direct sunlight. However, for the application to the standard installation (non-concentration), we must count the energy generation in the partially clear-sky days and cloudy days. A new idea of approximation of the all-climate spectrum model was developed and tried to this study and successfully modeled the energy yield of the tandem cells in all climates.

The advantage of the 4T configuration of the photovoltaic module using a triple-junction solar cell, precisely, InGaP/GaAs on Si solar cell, was compared by conventional 2T triple-junction module, specifically, InGaP/GaAs/InGaAs solar cell. The behavior of seasonal variation of performance and spectrum influence was modeled and validated outdoor measurement.

The annual amplitude of the seasonal peak-to-peak performance ratio improved by about 40 %. This robust performance of the seasonal fluctuation of the solar spectrum is useful to applications to high-performance photovoltaic applications like zero-emission buildings and light-weight aerospace [110]. For the use to the vehicle-integrated photovoltaic, it is also essential to consider 3D Solar Irradiance (modeling [111] and measurement [112]), as well as the performance of the photovoltaic in the curved surface (modeling [113] and the standard [114]).

The seasonal fluctuation of the 2-terminal triple-junction solar is also responsible for seasonal variation of the water precipitation. The above-validated model was expanded to various climate zones. The advantage of 4T on Si configuration increases (subarctic zone) < (temperate zone) < (subtropical zone).

It is important to note that the model we developed and validated is not only applied 4T InGaP/GaAs on Si solar cell, but can be extended to every type of the tandem solar cells in principle, including Perovskite on Si, Perovskite on CIGS, Polymer tandem, III-V tandem regardless of monolithic, wafer-bonding and mechanical stack. It even can be applied the partial concentrator tandem cells [78] and the super-multi-junction solar cells [1].

Author Contributions: Conceptualization: Y.O., and K.A.; methodology: H.T., H.S., Y.O., and K.A.; validation: H.T., H.S., T.T., Y.O., and K.A.; formal analysis: H.T., H.S., and Y.O.; data curation, H.T., H.S., and Y.O.; writing—original draft preparation, H.T., K.A. and Y.O.; writing—review and editing: H.T., Y.O., and K.A.; supervision: K.N. and M.Y. All authors have read and agreed to the published version of the manuscript.

Funding: This research was funded by the New Energy and Industrial Technology Development Organization (NEDO), and a grant for Scientific Research on Priority Areas from the University of Miyazaki.

Acknowledgments: This work was supported in part by the New Energy and Industrial Technology Development Organization (NEDO).

Conflicts of Interest: The authors declare that there are no conflicts of interest.

References

1. Araki, K.; Ota, Y.; Saiki, H.; Tawa, H.; Nishioka, K.; Yamaguchi, M. Super-Multi-Junction Solar Cells—Device Configuration with the Potential for More Than 50% Annual Energy Conversion Efficiency (Non-Concentration). *Appl. Sci.* **2019**, *9*, 4598.

2. Ekins-Daukes, N.J.; Betts, T.R.; Kemmoku, Y.; Araki, K.; Lee, H.S.; Gottschalg, R.; Boreland, M.B.; Infield, D.G.; Yamaguchi, M. Syracuse-a multi-junction concentrator system computer model. In Proceedings of the Conference Record of the Thirty-First IEEE Photovoltaic Specialists Conference, Lake Buena Vista, FL, USA, 3–7 January 2005; pp. 651–654.

3. Cameron, C.; Crawford, C.; Foresi, J.; King, D.; McConnell, R.; Riley, D.; Sahm, A.; Stein, J. Performance Model Assessment for Multi-Junction Concentrating Photovoltaic Systems. *Aip Conf. Proc.* **2010**, *1277*, 290–293.

4. Araki, K; Yamaguchi, M. Influences of spectrum change to 3-junction concentrator cells. *Solar energy materials and solar cells*. *2003* Feb 1;75(3-4):707-14.

5. Cai, Y.; Wang, W.W.; Liu, C.W.; Ding, W.T.; Liu, D.; Zhao, F.Y. Performance evaluation of a thermoelectric ventilation system driven by the concentrated photovoltaic thermoelectric generators for green building operations. *Renew. Energy* **2020**, *147*, 1565–1583.

6. Richter, A.; Hermle, M.; Glunz, S.W. Reassessment of the limiting efficiency for crystalline silicon solar cells. *IEEE Journal of Photovoltaics* **2013**, *3*, 1184–1191.

7. Jackson, E.D. Areas for Improving of the Semiconductor Solar Energy Converter. In Proceedings of the Transzation Conference on the Use of Solar Energy, Tucson, AZ, USA, 31 October–1 November 1955; University of Arizona Press: Tucson, AZ, USA, 1958; Volume 5, pp. 122–126.

8. Wolf, M. Limitations and possibilities for improvement of photovoltaic solar energy converters. *Proc. Inst. Radio Eng.* **1960**, *48*, 1246–1263.

9. Hutchby, J.A.; Markunas, R.J.; Timmons, M.L.; Chiang, P.K.; Bedair, S.M. A Review of Multijunction Concentrator Solar Cells. In Proceedings of the 18th IEEE Photovoltaic Specialists Conference, Las Vegas, NV, USA, 21–25 October 1985; IEEE: New York, NY, USA, 1985; pp. 20–27.

10. Ludowise, M.J.; LaRue, R.A.; Borden, P.G.; Gregory, P.E.; Dietz, W.T. High-efficiency organometallic vapor phase epitaxy AlGaAs/GaAs monolithic cascade solar cell using metal interconnects. *Appl. Phys. Lett.* **1982**, *41*, 550–552.

11. Flores, C. A three-terminal double junction GaAs/GaAlAs cascade solar cells. *IEEE Electron. Device Lett.* **1983**, EDL–4, 96–99.

12. Chung, B.C.; Virshup, G.F.; Hikido, S.; Kaminar, N.R. 27.6% efficiency (1 Sun, air mass 1.5) monolithic Al0.37 Ga0.63 As/GaAs two-junction cascade solar cell with prismatic cover glass. *Appl. Phys. Lett.* **1989**, *55*, 1741–1743.

13. Fan, J.C.C.; Tsaur, B.Y.; Palm, B.J. Optical Design of High-Efficiency Multi-Junction Cells. In Proceedings of the 16th IEEE Photovoltaic Specialists Conference, San Diego, CA, USA, 27–30 September 1982; IEEE: New York, NY, USA, 1982; pp. 692–701.

14. Yamaguchi, M.; Amano, C.; Sugiura, H.; Yamamoto, A. High efficiency AlGaAs/GaAs multi-junction solar cells. In Proceedings of the 19th IEEE Photovoltaic Specialists Conference, New Orleans, LA, USA, 4–8 May 1987; IEEE: New York, NY, USA, 1987; pp. 1484–1485.

15. Ando, K.; Amano, C.; Sugiura, H.; Yamaguchi, M.; Saletesm, A. Non-radiative e-h recombination characteristics of mid-gap electron trap in AlxGa1–x As (x = 0.4) grown by molecular beam epitaxy. *Jpn. J. Appl. Phys.* **1987**, *26*, L266–L269.

16. Sugiura, H.; Amano, C.; Yamamoto, A.; Yamaguchi, M. Double hetero¬structure GaAs tunnel junction for AlGaAs/GaAs multi-junction solar cells. *Jpn. J. Appl. Phys.* **1988**, *27*, 269–272.

17. Olson, J.M.; Kurtz, S.R.; Kibbler, A.E. A 27.3% efficient Ga0.5In0.5P/ GaAs multi-junction solar cell. *Appl. Phys. Lett.* **1990**, *56*, 623–625.

18. Bertness, K.A.; Kurtz, S.R.; Friedman, D.J.; Kibbler, A.E.; Kramer, C.; Olson, J.M. 29.5%-efficiency GaInP/GaAs multi-junction solar cells. *Appl. Phys. Lett.* **1994**, *65*, 989–991.

19. Sasaki, K.; Agui, T.; Nakaido, K.; Takahashi, N.; Onitsuka, R.; Takamoto, T. Development of InGaP/GaAs/InGaAs inverted triple junction concentrator solar cells. *Aip Conf. Proc.* **2013**, *1556*, 22–25.

20. Chiu, P.T.; Law, D.L.; Woo, R.L.; Singer, S.; Bhusari, D.; Hong, W.D.; Zakaria, A.; Boisvert, J.C.; Mesropian, S.; King, R.R.; et al. 35.8% space and 38.8% terrestrial 5J direct bonded cells. In Proceedings of the 40th IEEE Photovoltaic Specialist Conference, Denver, CO, USA, 8–13 June 2014; pp. 11–13.

21. Yamaguchi, M.; Lee, K.-H. ;Araki, K.; and Kojima, N. *J. Phys. D. Appl. Phys.* **2018**, *51*, 133002.

22. Essig, S.; Allebe, C.; Remo, T.; Geisz, T. F.; Steiner, M. A.; Horowitz, K.; Barrud, L.; Ward, J. S.; Schnabel, M.; Descoeudres, A.; Young, D. L.; Woodhouse, M.; Despeisse, M.; Ballif, C.; Tamboli, A. Raising the one-sun conversion efficiency of III–V/Si solar cells to 32.8% for two junctions and 35.9% for three junctions. *Nat. Energy,* **2017**, *2*, 17144.

23. Green, M. A.; Dunlop, E. D.; Levi, D. H.; Hohl-Ebinger, J.; Yoshita, M.; Ho-Baillie, A. W. Y. Solar cell efficiency tables (version 54). *Prog. Photovoltaics* **2019**, *27*, 565.

24. Carmody, M.; Mallick, S.; Margetis, J.; Kodama, R.; Biegala, T.; Xu, D.; Bechmann, P.; Garland, J. W.; Sivananthan, S. Single-crystal II-VI on Si single-junction and tandem solar cells. *Appl. Phys. Lett.* **2010**, *96*, 153502.

25. Yao, M.; Cong, S.; Arab, S.; Huang, N.; Povinelli, M. L.; Cronin, S. B.; Dapkus, P. D.; Zhou, C. Tandem solar cells using GaAs nanowires on Si: design, fabrication, and observation of voltage addition. *Nano Lett.* **2015**, *15*, 7217.

26. Araki. K.; Ota, Y.; Lee, KH.; Nishioka, K.; Yamaguchi, M. Is it CPV? Yes, but it is a partial CPV. In AIP Conference Proceedings 2017 Sep 6 (Vol. 1881, No. 1, p. 080001). AIP Publishing LLC.

27. Araki, K.; Lee, KH.; Yamaguchi, M. The possibility of the static LCPV to mechanical-stack III-V//Si module. InAIP Conference Proceedings 2018 Sep 13 (Vol. 2012, No. 1, p. 090002). AIP Publishing LLC.

28. Sato, D.; Lee, KH.; Araki, K.; Masuda, T.; Yamaguchi, M.; Yamada, N. Design and Evaluation of Low-concentration Static III-V/Si Partial CPV Module for Car-rooftop Application. In2018 IEEE 7th World Conference on Photovoltaic Energy Conversion (WCPEC)(A Joint Conference of 45th IEEE PVSC, 28th PVSEC & 34th EU PVSEC) 2018 Jun 10 (pp. 0954-0957). IEEE.

29. Takamoto, T.; Washio, H.; Juso, H. Application of InGaP/GaAs/InGaAs triple junction solar cells to space use and concentrator photovoltaic. In Proceedings of the 2014 IEEE 40th Photovoltaic Specialist Conference (PVSC), Denver, CO, USA, 8–13 June 2014; pp. 1–5.

30. Löper, P.; Moon, S. J.; De Nicolas, S. M.; Niesen, B.; Ledinsky, M.; Nicolay, S.; Bailat, J.; Yum, J. H.; De Wolf, S.; Ballif, C.; Organic–inorganic halide perovskite/crystalline silicon four-terminal tandem solar cells. *Physical Chemistry Chemical Physics*. **2015**,17(3), 1619-29.

31. Schneider, BW.; Lal, N. N.; Baker-Finch, S.; White, T. P.; Pyramidal surface textures for light trapping and antireflection in perovskite-on-silicon tandem solar cells. *Optics express*. **2014** Oct 20, 22(106), A1422-30.

32. Werner, J; Sahli, F.; Fu, F.; Diaz, Leon, J. J.; Walter, A.; Kamino, B. A.; Niesen, B.; Nicolay, S.; Jeangros, Q.; Ballif, C. Perovskite/perovskite/silicon monolithic triple-junction solar cells with a fully textured design. *ACS Energy Letters*. **2018** Aug 3, 3(9), 2052-8.

33. Sahli, F.; Werner, J.; Kamino, B. A.; Bräuninger, M.; Monnard, R.; Paviet-Salomon, B.; Barraud, L.; Ding, L.; Leon, J. J.; Sacchetto, D.; Cattaneo, G. Fully textured monolithic perovskite/silicon tandem solar cells with 25.2% power conversion efficiency. *Nature materials*. **2018** Sep, 17(9), 820-6.

34. Hörantner, M. T.; Snaith, H. J.; Predicting and optimising the energy yield of perovskite-on-silicon tandem solar cells under real world conditions. *Energy & Environmental Science*. **2017**, 10(9), 1983-93.

35. Ishii, T.; Otani, K.; Takashima, T.; Xue, Y. Solar spectral influence on the performance of photovoltaic (pv) modules under fine weather and cloudy weather conditions. Prog. Photovoltaics 2013, 21, 481–489.

36. Araki, K.; Yamaguchi, M. Influences of spectrum change to 3-junction concentrator cells. *Sol. Energy Mater. Sol. Cells* **2003**, *75*, 707–714.

37. Faine, P.; Kurtz, S.R.; Riordan, C.; Olson, J.M. The influence of spectral solar irradiance variations on the performance of selected single-junction and multijunction solar cells. *Solar Cells* **1991**, *31*, 259–278.

38. Kirn, B.; Topic, M. Diffuse and direct light solar spectra modeling in pv module performance rating. *Sol. Energy* **2017**, *150*, 310–316.

39. Nofuentes, G.; García-Domingo, B.; Muñoz, J.V.; Chenlo, F. Analysis of the dependence of the spectral factor of some pv technologies on the solar spectrum distribution. *Appl. Energy* **2014**, *113*, 302–309.

40. Alonso-Abella, M.; Chenlo, F.; Nofuentes, G.; Torres-Ramírez, M. Analysis of spectral effects on the energy yield of different pv (photovoltaic) technologies: The case of four specific sites. *Energy* **2014**, *67*, 435–443.

41. Philipps, S.P.; Bett, A.W.; Horowitz, K.; Kurtz, S. Current Status of Concentrator Photovoltaic (CPV) Technology; Version 1.3; National Renewable Energy Lab NREL: Lakewood, CO, USA, **2017**; pp. 10–11.

42. Araki, K.; Yamaguchi, M. Influences of spectrum change to 3-junction concentrator cells. *Sol. Energy Mater. Sol. Cells* **2003**, 75, 707–714.

43. Faine, P.; Kurtz, S.R.; Riordan, C.; Olson, J.M. The influence of spectral solar irradiance variations on the performance of selected single-junction and multijunction solar cells. *Sol. Cells* **1991**, 31, 259–278.

44. Kurtz, S.R.; Olson, J.M.; Faine, P. The difference between standard and average efficiencies of multijunction compared with single-junction concentrator cells. *Solar Cells* **1991**, 30, 501–513.

45. Philipps, S.P.; Peharz, G.; Hoheisel, R.; Hornung, T.; Al-Abbadi, N.M.; Dimroth, F.; Bett, A.W. Energy harvesting efficiency of III–V triple-junction concentrator solar cells under realistic spectral conditions. *Sol. Energy Mater. Sol. Cells* **2010**, 94, 869–877.

46. Kinsey, G.S.; Edmondson, K.M. Spectral response and energy output of concentrator multijunction solar cells. *Prog. Photovolt. Res. Appl.* **2009**, 17, 279–288.

47. Araki, K.; Emery, K.; Siefer, G.; Bett, A.W.; Sakakibara, T.; Kemmoku, Y.; Ekins-Daukes, N.J.; Lee, H.S.; Yamaguchi, M. Comparison of efficiency measurements for a HCPV module with 3J cells in 3 sites. In Proceedings of the Conference Record of the Thirty-First IEEE Photovoltaic Specialists Conference, Lake Buena Vista, FL, USA, 3–7 January 2005; pp. 846–849.

48. Lee, H.S.; Ekins-Daukes, N.J.; Araki, K.; Kemmoku, Y.; Yamaguchi, M. Field test and analysis: The behavior of 3-J concentrator cells under the control of cell temperature. In Proceedings of the Conference Record of the Thirty-First IEEE Photovoltaic Specialists Conference, Lake Buena Vista, FL, USA, 3–7 January 2005; pp. 754–757.

49. Al Husna, H.; Ota, Y.; Minemoto, T.; Nishioka, K. Field test analysis of concentrator photovoltaic system focusing on average photon energy and temperature. Jpn. J. Appl. Phys. 2015, 54, 08KE05.

50. Verlinden, P.J.; Lasich, J.B. Energy rating of concentrator PV systems using multi-junction III–V solar cells. In Proceedings of the 33rd IEEE Photovoltaic Specialists Conference, San Diego, CA, USA, 11–16 May 2008; pp. 1–6.

51. Victoria, M.; Askins, S.; Nuñez, R.; Domínguez, C.; Herrero, R.; Antón, I.; Sala, G.; Ruíz, J.M. Tuning the current ratio of a CPV system to maximize the energy harvesting in a particular location. *Aip Conf. Proc.* **2013**, 1556, 156–161.

52. Muller, M.; Marion, B.; Kurtz, S.; Rodriguez, J. An investigation into spectral parameters as they impact CPV module performance. *Aip Conf. Proc.* **2010**, 1277, 307–311.

53. Domínguez, C.; Antón, I.; Sala, G.; Askins, S. Current-matching estimation for multijunction cells within a CPV module by means of component cells. *Prog. Photovolt. Res. Appl.* **2013**, 21, 1478–1488.

54. Núñez, R.; Jin, C.; Antón, I.; Sala, G. Spectral classification of worldwide locations using SMR indexes. *Aip Conf. Proc.* **2016**, 1766, 090007.

55. Araki, K.; Yamaguchi, M.; Kondo, M.; Uozumi, H. Which is the best number of junctions for solar cells under ever-changing terrestrial spectrum? In Proceedings of the 3rd World Conference on Photovoltaic Energy Conversion, Osaka, Japan, 11–18 May 2003; pp. 307–310.

56. Letay, G.; Baur, C.; Bett, A. Theoretical investigations of III-V multi-junction concentrator cells under realistic spectral conditions. In Proceedings of the 19th European Photovoltaic Solar Energy Conference, Paris, France, 7–11 June 2004; p. 11.

57. Ekins-Daukes, N.J.; Kemmoku, Y.; Araki, K.; Betts, T.R.; Gottschalg, R.; Infield, D.G.; Yamaguchi, M. The design specification for syracuse; a multi-junction concentrator system computer model. In Proceedings of the 19th European Photovoltaic Solar Energy Conference, Paris, France, 7–11 June 2004.

58. Cameron, C.; Crawford, C.; Foresi, J.; King, D.; McConnell, R.; Riley, D.; Sahm, A.; Stein, J. Performance Model Assessment for Multi-Junction Concentrating Photovoltaic Systems. *Aip Conf. Proc.* **2010**, 1277, 290–293.

59. Araki, K.; Uozumi, H.; Kondo, M.; Takamoto, T.; Agui, T.; Kaneiwa, M.; Egami, T.; Hiramatsu, M.; Miyazaki, Y.; Kemmoku, Y.; et al. Development of a new 550/spl times/concentrator module with 3J cells-performance and reliability. In Proceedings of the Conference Record of the Thirty-First IEEE Photovoltaic Specialists Conference, Lake Buena Vista, FL, USA, 3–7 January 2005; pp. 631–634.

60. Araki, K.; Yamaguchi, M. Extended distributed model for analysis of non-ideal concentration operation. *Sol. Energy Mater. Sol. Cells* **2003**, 75, 467–473.

61. Herrero, R.; Victoria, M.; Domínguez, C.; Askins, S.; Antón, I.; Sala, G. Concentration photovoltaic optical system irradiance distribution measurements and its effect on multi-junction solar cells. *Prog. Photovolt. Res. Appl.* **2012**, 20, 423–430.

62. Garcia, I.; Algora, C.; Rey-Stolle, I.; Galiana, B. Study of non-uniform light profiles on high concentration III–V solar cells using quasi-3D distributed models. In Proceedings of the 33rd IEEE Photovoltaic Specialists Conference, San Diego, CA, USA, 11–16 May 2008; pp. 1–6.

63. Kurtz, S.R.; O'Neill, M.J. Estimating and controlling chromatic aberration losses for two-junction, two-terminal devices in refractive concentrator systems. In Proceedings of the Conference Record of the Twenty Fifth IEEE Photovoltaic Specialists Conference, Washington, DC, USA, 13–17 May 1996; pp. 361–364.

64. James, L.W. Effects of concentrator chromatic aberration on multi-junction cells. In Proceedings of the 1994 IEEE 1st World Conference on Photovoltaic Energy Conversion-WCPEC (A Joint Conference of PVSC, PVSEC and PSEC), Waikoloa, HI, USA, 5–9 December 1994; pp. 1799–1802.

65. Rey-Stolle, I.; Algora, C.; García, I.; Baudrit, M.; Espinet, P.; Galiana, B.; Barrigón, E. Simulating III–V concentrator solar cells: A comparison of advantages and limitations of lumped analytical models; distributed analytical models and numerical simulation. In Proceedings of the 34th IEEE Photovoltaic Specialists Conference (PVSC), Philadelphia, PA, USA, 7–12 June 2009; pp. 001622–001627.

66. Herrero, R.; Askins, S.; Antón, I.; Sala, G.; Araki, K.; Nagai, H. Module optical analyzer: Identification of defects on the production line. *Aip Conf. Proc.* **2014,** 1616, 119-123.

67. Araki, K.; Nagai, H.; Herrero, R.; Antón, I.; Sala, G.; Yamaguchi, M. Off-Axis Characteristics of CPV Modules Result From Lens-Cell Misalignment—Measurement and Monte Carlo Simulation. *IEEE Journal of Photovoltaics.* **2016** Jul 28, 6(5), 1353-9.

68. Araki, K.; Herrero, R.; Antón, I.; Sala, G.; Nagai, H.; Lee, K. H.; Yamaguchi, M. Why are acceptance angle of P m and Isc different in spite of uniform illumination onto concentrator solar cells?. In2016 IEEE 43rd Photovoltaic Specialists Conference (PVSC) 2016 Jun 5 (pp. 0549-0553). IEEE.

69. Araki, K.; Nagai, H.; Herrero, R.; Antón, I.; Sala, G.; Lee, K. H.; Yamaguchi, M. 1-D and 2-D Monte Carlo simulations for analysis of CPV module characteristics including the acceptance angle impacted by assembly errors. *Solar Energy.* **2017** May 1, 147, 448-54.

70. Saiki, H.; Sakai, T.; Araki, K.; Ota, Y.; Lee, K. H.; Yamaguchi, M.; Nishioka, K. Verification of uncertainty in CPV's outdoor performance. In2018 IEEE 7th World Conference on Photovoltaic Energy Conversion (WCPEC)(A Joint Conference of 45th IEEE PVSC, 28th PVSEC & 34th EU PVSEC) 2018 Jun 10 (pp. 0949-0953). IEEE.

71. Araki, K.; Ota, Y.; Sakai, T.; Lee, K. H.; Yamaguchi, M. Inherent uncertainty of energy ratings of multi-junction cells by the fluctuation of atmospheric parameters. Proceedings of the PVSEC-27, Otsu, Japan. 2017 Nov:12-7.

72. Ota, Y.; Masuda, T.; Araki, K.; Yamaguchi, M. A mobile multipyranometer array for the assessment of solar irradiance incident on a photovoltaic-powered vehicle. *Sol. Energy* **2019**, 184, 84–90.

73. Ota, Y.; Nishioka, K.; Araki, K.; Ikeda, K.; Lee, K.H.; Yamaguchi, M. Optimization of static concentrator photovoltaics with aspherical lens for automobile. In Proceedings of the IEEE 43rd Photovoltaic Specialists Conference (PVSC), Portland, OR, USA, 5–10 June 2016; pp. 0570–0573.

74. Araki, K.; Ota, Y.; Ikeda, K.; Lee, K.H.; Nishioka, K.; Yamaguchi, M. Possibility of static low concentrator PV optimized for vehicle installation. *Aip Conf. Proc.* **2016**, 1766, 020001.

75. Araki, K.; Nagai, H.; Yamaguchi, M. Possibility of solar station to EV. *Aip Conf. Proc.* **2016**, 1766, 080001.

76. Schuss, C.; Gall, H.; Eberhart, K.; Illko, H.; Eichberger, B. Alignment and interconnection of photovoltaics on electric and hybrid electric vehicles. In Proceedings of the 2014 IEEE International Instrumentation and Measurement Technology Conference (I2MTC) Proceedings, Montevideo, Uruguay, 12–15 May 2014; pp. 153–158.

77. Schuss, C.; Eichberger, B.; Rahkonen, T. Impact of sampling interval on the accuracy of estimating the amount of solar energy. In Proceedings of the IEEE International Instrumentation and Measurement Technology Conference Proceedings, Taipei, Taiwan, 23–26 May 2016; pp. 1–6.

78. Sato, D.; Lee, K.H.; Araki, K.; Masuda, T.; Yamaguchi, M.; Yamada, N. Design of low-concentration static III-V/Si partial CPV module with 27.3% annual efficiency for car-roof application. *Prog. Photovolt. Res. Appl.* **2019**, 27, 501–510.

79. Sato, D.; Lee, K.H.; Araki, K.; Masuda, T.; Yamaguchi, M.; Yamada, N. Design and Evaluation of Low-concentration Static III-V/Si Partial CPV Module for Car-rooftop Application. In Proceedings of the IEEE 7th World Conference on Photovoltaic Energy Conversion (WCPEC) (A Joint Conference of 45th IEEE PVSC, 28th PVSEC & 34th EU PVSEC), Waikoloa Village, HI, USA, 10–15 June 2018; pp. 0954–0957.

80. Masuda, T.; Araki, K.; Okumura, K.; Urabe, S.; Kudo, Y.; Kimura, K.; Nakado, T.; Sato, A.; Yamaguchi, M. Next environment-friendly cars: Application of solar power as automobile energy source. In Proceedings of the 2016 IEEE 43rd Photovoltaic Specialists Conference (PVSC), Portland, OR, USA, 5–10 June 2016; pp. 0580–0584.

81. Araki, K.; Algora, C.; Siefer, G.; Nishioka, K.; Leutz, R.; Carter, S.; Wang, S.; Askins, S.; Ji, L.; Kelly, G. Standardization of the CPV and car-roof PV technology in 2018–Where are we going to go? *Aip Conf. Proc.* **2018**, 2012, 070001.

82. Araki, K.; Algora, C.; Siefer, G.; NIshioka, K.; Muller, M.; Leutz, R.; Carter, S.; Wang, S.; Askins, S.; Ji, L.; et al. Toward Standardization of Solar trackers, concentrator PV, and car-roof PV. Grand Renew. Energy Proc. Jpn. Counc. Renew. Energy 2018, 2018, 37.

83. Araki, K.; Lee, K.H.; Yamaguchi, M. The possibility of the static LCPV to mechanical-stack III-V//Si module. *Aip Conf. Proc.* **2018**, 2012, 090002.

84. Ota, Y.; Masuda, T.; Araki, K.; Yamaguchi, M. Curve-correction factor for characterization of the output of a three-dimensional curved photovoltaic module on a car roof. *Coatings* **2018**, 8, 432.

85. Araki, K.; Kemmoku, Y.; Yamaguchi, M. A simple rating method for CPV modules and systems. In Proceedings of the 33rd IEEE Photovoltaic Specialists Conference, San Diego, CA, USA, 11–16 May 2008; pp. 1–6.

86. Araki, K.; Lee, K.H.; Yamaguchi, M. Impact of the atmospheric conditions to the bandgap engineering of multi-junction cells for optimization of the annual energy yield of CPV. *Aip Conf. Proc.* **2017**, 1881, 070002.

87. Cariou, R.; Benick, J.; Feldmann, F.; Höhn, O.; Hauser, H.; Beutel, P.; Razek, N.; Wimplinger, M.; Bläsi, B.; Lackner, D.; Hermle, M.; Siefer, G.; Glunz, S.W.; Bett, A.W.; Dimroth, F. III–V-on-silicon solar cells reaching 33% photoconversion efficiency in two-terminal configuration. *Nature Energy* **2018**, *3*, 326-333.

88. Araki, K.; Ota, Y.; Lee, K. H.; Nishioka, K.; Yamaguchi, M. CPV Technologies Not Relying on Perfection of Trackers. In2017 IEEE 44th Photovoltaic Specialist Conference (PVSC) 2017 Jun 25 (pp. 1479-1484). IEEE.

89. Masuda, T.; Araki, K.; Okumura, K.; Urabe, S.; Kudo, Y.; Kimura, K.; Nakado, T.; Sato, A.; Yamaguchi, M. Static concentrator photovoltaics for automotive applications. *Solar Energy*. **2017** Apr 1, 146, 523-31.

90. Lee, K. H.; Araki, K.; Ota, Y.; Nishioka, K.; Yamaguchi, M. Quantifying the potential of III-V/Si partial concentrator by a statistical approach. *Aip Conf. Proc.* **2017**, 1881, 1, 080007.

91. Araki, K.; Ota, Y.; Lee, K. H.; Nishioka, K.; Yamaguchi, M. Design of the partial concentrator lens for III-V on Si static concentration. *Aip Conf. Proc.* **2017,** 1881, 1, 030001.

92. Ota, Y.; Araki, K.; Lee, K. H.; Yamaguchi, M.; Nishioka, K. Estimation of conversion efficiency for partially static concentrator with III-V on Si solar cell. *Aip Conf. Proc.* **2017,** 1881, 1, 020010.

93. Nagashima, T.; Okumura, K.; Murata, K.; Kimura, Y. Three-terminal tandem solar cells with a back-contact type bottom cell. In Conference Record of the Twenty-Eighth IEEE Photovoltaic Specialists Conference-2000 (Cat. No. 00CH37036) 2000 Sep 15 (pp. 1193-1196). IEEE.

94. Sista, S.; Hong, Z.; Park, M. H.; Xu, Z.; Yang, Y. High-efficiency polymer tandem solar cells with three-terminal structure. *Advanced Materials*. **2010**, 22(8), E77-80.

95. Steiner, M. A.; Wanlass, M. W.; Carapella, J. J.; Duda, A.; Ward, J. S.; Moriarty, T. E.; Emery, K. A. A monolithic three-terminal GaInAsP/GaInAs tandem solar cell. *Progress in Photovoltaics: Research and Applications*. **2009,** 17(8), 587-93.

96. Soga, T.; Yang, M.; Jimbo, T.; Umeno, M. High-efficiency monolithic three-terminal GaAs/Si tandem solar cells fabricated by metalorganic chemical vapor deposition. *Japanese journal of applied physics*. **1996** ,35(2S), 1401.

97. Wang, L.; Conrad, B.; Soeriyadi, A.; Zhao, X.; Li, D.; Diaz, M.; Lochtefeld, A.; Gerger, A.; Perez-Wurfl, I.; Barnett, A. Current matched three-terminal dual junction GaAsP/SiGe tandem solar cell on Si. *Solar Energy Materials and Solar Cells*. **2016** 1, 146, 80-6.

98. Bird, R.E.; Riordan, C. Simple solar spectral model for direct and diffuse irradiance on horizontal and tilted planes at the earth's surface for cloudless atmospheres. *Journal of Climate & Applied Meteorology* **1986**, *25*, 87–97.

99. Tawa, H.; Saiki, H.; Ota, Y.; Araki, K.; Takamoto, T.; Nishioka, K. Accurate Output Forecasting Method for Various Photovoltaic Modules Considering Incident Angle and Spectral Change Owing to Atmospheric Parameters and Cloud Conditions. *Appl. Sci.* **2020**, *10*, 703.

100. Araki, K.; Ota, Y.; Sakai, T.; Lee, K.H.; Nishioka, K.; Yamaguchi, M. Energy yield prediction of multi-junction cells considering atmospheric parameters fluctuation using Monte Carlo methods. In Proceedings of the PVSEC-27, Otsu, Japan, 12–17 November 2017.

101. Araki, K.; Ota, Y.; Sakai, T.; Lee, K.H.; Yamaguchi, M. Inherent uncertainty of energy ratings of multi-junction cells by the fluctuation of atmospheric parameters. In Proceedings of the PVSEC-27, Otsu, Japan, 12–17 November 2017.

102. Araki, K.; Ota, Y.; Lee, K. H.; Sakai, T.; Nishioka, K.; Yamaguchi, M. Analysis of fluctuation of atmospheric parameters and its impact on performance of CPV. *Aip Conf. Proc.* **2018,** 2012, 1, 080002.

103. Araki, K.; Yamaguchi, M.; Takamoto, T.; Ikeda, E.; Agui, T.; Kurita, H.; Takahashi, K.; Unno, T. Characteristics of GaAs-based concentrator cells. *Solar energy materials and solar cells.* **2001**, 66(1-4), 559-65.

104. Araki, K.; Yamaguchi, M. Extended distributed model for analysis of non-ideal concentration operation. *Solar energy materials and solar cells.* **2003**, 75(3-4), 467-73.

105. Saiki, H.; Sakai, T.; Araki, K.; Ota, Y.; Lee, K. H.; Yamaguchi, M.; Nishioka, K. Verification of uncertainty in CPV's outdoor performance. In 2018 IEEE 7th World Conference on Photovoltaic Energy Conversion (WCPEC)(A Joint Conference of 45th IEEE PVSC, 28th PVSEC & 34th EU PVSEC) 2018 Jun 10 (pp. 0949-0953). IEEE.

106. Itagaki, A.; Okumura, H.; Yamada, A. Preparation of meteorological data set throughout Japan for suitable design of PV systems Photovoltaic Energy Conversion. In Proceedings of the 3rd World Conference on Photovoltaic Energy Conversion, Osaka, Japan, 11–18 May 2003; Volume 2.

107. Shirakawa, K.; Itagaki, A.; Utsunomiya, T. Preparation of hourly solar radiation data on inclined surface (METPV-11) throughout Japan. In Proceedings of the JSES/JWEA Joint Conference, Wakkanai, Japan, 21–22 September 2011; pp. 193–196.

108. Araki, K.; Ota, Y.; Lee, K. H.; Nishioka, K.; Yamaguchi, M. Improvement of the spectral sensitivity of CPV by enhancing luminescence coupling and fine-tuning to the bottom-bandgap matched to local atmospheric conditions. *Aip Conf. Proc.* **2019**, 2149, 1, 060001.

109. Araki, K.; Ota, Y.; Lee, K. H.; Nishioka, K.; Yamaguchi M. Super-Multi-Junction Solar Cells, a New Configuration of the Robust and High-Efficiency Solar Cell and Its Application–Operation Model Based on the Annual Monitoring of the Multi-Junction PV Modules. In 2019 18th International Conference on Optical Communications and Networks (ICOCN) 2019 Aug 5 (pp. 1-3). IEEE.

110. Araki, K.; Ji, L.; Kelly, G.; Yamaguchi, M. To Do List for Research and Development and International Standardization to Achieve the Goal of Running a Majority of Electric Vehicles on Solar Energy. *Coatings* **2018**, 8, 251.

111. Araki, K.; Ota, Y.; Yamaguchi, M. Measurement and Modeling of 3D Solar Irradiance for Vehicle-Integrated Photovoltaic. *Appl. Sci.* **2020**, 10, 872.

112. Ota, Y.; Masuda, T.; Araki, K.; Yamaguchi, M. A mobile multipyranometer array for the assessment of solar irradiance incident on a photovoltaic-powered vehicle. *Solar Energy.* **2019**, 184, 84-90.

113. Ota, Y.; Masuda, T.; Araki, K.; Yamaguchi, M. Curve-correction factor for characterization of the output of a three-dimensional curved photovoltaic module on a car roof. *Coatings.* **2018** 8(12), 432.

114. Tayagaki, T.; Araki, K.; Yamaguchi, M.; Sugaya, T. Impact of Nonplanar Panels on Photovoltaic Power Generation in the Case of Vehicles. IEEE Journal of Photovoltaics. 2019 Sep 23;9(6):1721-6.

115. Araki, K.; Algora, C.; Siefer, G.; Nishioka, K.; Leutz, R.; Carter, S.; Wang, S.; Askins, S.; Ji, L.; Kelly, G. Standardization of the CPV and Car-roof PV Technology in 2018–Where are We Going to Go?. *Aip Conf. Proc.* **2018**, 2012, 1, 070001.